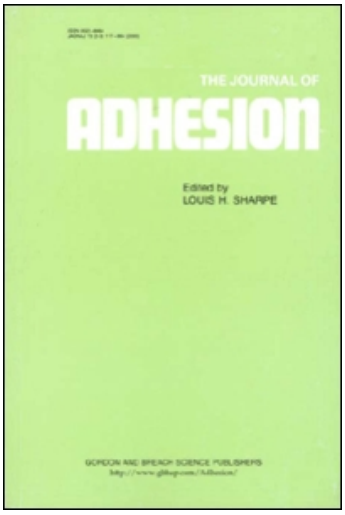


## The Journal of Adhesion

Publication details, including instructions for authors and subscription information:
http://www.informaworld.com/smpp/title~content=t713453635

# Unifying Design Strategies in Demosponge and Hexactinellid Skeletal Systems

James C. Weaver[a]; Garrett W. Milliron[a]; Peter Allen[b]; Ali Miserez[c]; Aditya Rawal[d]; Javier Garay[e]; Philipp J. Thurner[f]; Jong Seto[g]; Boaz Mayzel[h]; Larry Jon Friesen[i]; Bradley F. Chmelka[d]; Peter Fratzl[g]; Joanna Aizenberg[j]; Yannicke Dauphin[k]; David Kisailus[a]; Daniel E. Morse[l]

[a] Department of Chemical and Environmental Engineering, University of California, Riverside, Riverside, CA, USA [b] Engineering Department, University of California, Santa Barbara, Santa Barbara, CA, USA [c] Materials Department and Department of Molecular, Cellular, and Developmental Biology, University of California, Santa Barbara, Santa Barbara, CA, USA [d] Department of Chemical Engineering, University of California, Santa Barbara, Santa Barbara, CA, USA [e] Department of Mechanical Engineering, Materials Science and Engineering Program, University of California, Riverside, Riverside, CA, USA [f] Bioengineering Science Research Group, School of Engineering Science, University of Southampton Highfield, Southampton, U.K. [g] Department of Biomaterials, Max Planck Institute of Colloids and Interfaces, Potsdam, Germany [h] Department of Zoology, Faculty of Life Sciences, Tel Aviv University, Tel Aviv, Israel [i] Department of Biological Sciences, Santa Barbara City College, Santa Barbara, CA, USA [j] School of Engineering and Applied Sciences, Department of Chemistry and Chemical Biology, Harvard University, Cambridge, MA, USA [k] UMR IDES, University of Paris-Sud, Orsay, France [l] Department of Molecular, Cellular and Developmental Biology, Institute for Collaborative Biotechnologies, Materials Research Laboratory, and California Nanosystems Institute, University of California, Santa Barbara, Santa Barbara, CA, USA

Online publication date: 05 February 2010

**To cite this Article** Weaver, James C. , Milliron, Garrett W. , Allen, Peter , Miserez, Ali , Rawal, Aditya , Garay, Javier , Thurner, Philipp J. , Seto, Jong , Mayzel, Boaz , Friesen, Larry Jon , Chmelka, Bradley F. , Fratzl, Peter , Aizenberg, Joanna , Dauphin, Yannicke , Kisailus, David and Morse, Daniel E.(2010) 'Unifying Design Strategies in Demosponge and Hexactinellid Skeletal Systems', The Journal of Adhesion, 86: 1, 72 — 95

**To link to this Article: DOI:** 10.1080/00218460903417917

**URL:** http://dx.doi.org/10.1080/00218460903417917

*The Journal of Adhesion*, 86:72–95, 2010

ISSN: 0021-8464 print/1545-5823 online
DOI: 10.1080/00218460903417917

Taylor & Francis
Taylor & Francis Group



# Unifying Design Strategies in Demosponge and Hexactinellid Skeletal Systems

**James C. Weaver[1], Garrett W. Milliron[1], Peter Allen[2], Ali Miserez[3], Aditya Rawal[4], Javier Garay[5], Philipp J. Thurner[6], Jong Seto[7], Boaz Mayzel[8], Larry Jon Friesen[9], Bradley F. Chmelka[4], Peter Fratzl[7], Joanna Aizenberg[10], Yannicke Dauphin[11], David Kisailus[1], and Daniel E. Morse[12]**

[1]Department of Chemical and Environmental Engineering, University of California, Riverside, Riverside, CA, USA
[2]Engineering Department, University of California, Santa Barbara, Santa Barbara, CA, USA
[3]Materials Department and Department of Molecular, Cellular, and Developmental Biology, University of California, Santa Barbara, Santa Barbara, CA, USA
[4]Department of Chemical Engineering, University of California, Santa Barbara, Santa Barbara, CA, USA
[5]Department of Mechanical Engineering, Materials Science and Engineering Program, University of California, Riverside, Riverside, CA, USA
[6]Bioengineering Science Research Group, School of Engineering Science, University of Southampton Highfield, Southampton, U.K.
[7]Department of Biomaterials, Max Planck Institute of Colloids and Interfaces, Potsdam, Germany
[8]Department of Zoology, Faculty of Life Sciences, Tel Aviv University, Tel Aviv, Israel
[9]Department of Biological Sciences, Santa Barbara City College, Santa Barbara, CA, USA

Received 6 March 2009; in final form 20 August 2009.

This article is dedicated to Professor J. Herbert Waite who continues to be an inspiration for investigating structure-function relationships in biological systems.

One of a Collection of papers honoring J. Herbert Waite, the recipient in February 2009 of *The Adhesion Society Award for Excellence in Adhesion Science, Sponsored by 3M*.

Address correspondence to David Kisailus, Department of Chemical and Environmental Engineering, University of California, Riverside, CA 92521, USA. E-mail: david@engr.ucr.edu or Daniel E. Morse, Department of Molecular, Cellular and Developmental Biology, University of California, Santa Barbara, CA 93106, USA. E-mail: d_morse@lifesci.ucsb.edu

[10]School of Engineering and Applied Sciences, Department of Chemistry and Chemical Biology, Harvard University, Cambridge, MA, USA
[11]UMR IDES, University of Paris-Sud, Orsay, France
[12]Department of Molecular, Cellular and Developmental Biology, Institute for Collaborative Biotechnologies, Materials Research Laboratory, and California Nanosystems Institute, University of California, Santa Barbara, Santa Barbara, CA, USA

*Biological systems are well known for their ability to construct remarkably complex and mechanically robust skeletal structures from a great diversity of minerals. One such example, silica, is widely used in the synthesis of skeletal elements (spicules) within the phylum Porifera (the sponges). As a result, members of this diverse group have served as useful model systems for analysis of the dynamic processes of biosilicification and for investigating structure function relationships in their often hierarchically ordered skeletal systems. This article describes in detail the skeletal diversity within the two silica-forming sponge classes, the Demospongiae and the Hexactinellida, and through the use of several representative examples, discusses the mechanical consequences of the various modes of construction implemented as well as the potential evolutionary pressures that resulted in their observed structural complexity.*

**Keywords:** Biomineralization; Biosilica; Composite; Fracture mechanics; Porifera



## INTRODUCTION

The diversity of silica skeletal systems in the phylum Porifera (the sponges) is truly remarkable [1–5]. Despite the nearly 200 years of scientific data available on the subject, however, there is no unified theory that can explain the observed complexity at the ultrastructural level of the individual spicules or the mechanisms and design principles by which they assemble to produce hierarchically organized skeletal networks.

The two main silicifying sponge classes, the Demospongiae and the Hexactinellida, differ significantly from one another with respect to spicule symmetry, structural diversity, and basic histology. While demosponges consist predominantly of loose aggregations of individual cells with specialized functions, the hexactinellids are principally composed of massive multinucleate syncytia[1] [5–7]. These differences

[1]A syncytium is a large cell-like mass of cytoplasm containing multiple nuclei and enclosed in a membrane with no internal cell boundaries. Syncytia frequently result from the fusion of two or more cells.

in histology have a dramatic effect on the dimensional limits of the spicules synthesized by members of these two sponge classes.

In demosponges, the maximum spicule size encountered is typically a few millimeters in total length [1,2]. This limitation is mainly related to the fundamental mechanisms, by which these spicules are formed. In these sponges, recent evidence suggests that the central axial filament that provides a substrate for early silica deposition is synthesized in its entirety prior to silicification [8]. As a result, the maximum dimensions of a single spicule are fundamentally limited by the extensibility of the individual cells involved in axial filament synthesis.

High-resolution structural analyses of demosponge spicules have revealed that the central axial filament is hexagonal, or some derivative thereof, in cross-section and is surrounded by concentric lamellae of consolidated silica nanoparticles [9,10]. While the silica surrounding the axial filament is deposited in layers exhibiting variability in the degree of silica condensation, there are no detectable quantities of organic matter present [9,10].



These general design strategies of demosponge spicules differ significantly from those seen in the hexactinellids. Whereas hexactinellid spicules also possess a proteinaceous axial filament, it is distinctly square in cross-section [11], in contrast to the hexagonal form found in demosponges [12–14]. The cross-sectional morphology of these axial filaments plays a direct role in establishing the unique three-axis (or six-rayed) geometry characteristic of the hexactinellid spicules. Lateral filament outgrowth from the four faces of the main central axis results in the formation of three distinct axes (two in addition to the central axis) that intersect one another at right angles. In addition to the unique axial filament morphology found in the hexactinellids, the mechanism of axial filament synthesis also appears to be distinct. Unlike demosponge axial filaments, which are synthesized in their entirety prior to silica deposition, those in the hexactinellids appear to grow continuously during spicule biosynthesis [15]. This central organic scaffold is reportedly connected to the surrounding syncytium *via* an opening in the end of each spicule ray, and once spicule lateral growth has ceased, the openings are sealed by the deposition of additional silica [4]. In addition to the growth potential of the axial filament, because of the syncytial nature of the sclerocytes, there is practically no limitation to the dimensions of the synthesized spicules.

The following discussion of sponge spicule architectural diversity is based on the observations obtained from a wide range of different demosponge and hexactinellid species. Because of the ultrastructural

simplicity of demosponge spicules outlined above (consisting of fused concentric lamellae of consolidated silica nanoparticles), they will be used as a comparative metric for the following analysis of hexactinellid skeletal diversity. Based on these observations, we attempt to explain the basic design features from a mechanics perspective in hopes of gaining additional insight into the potential evolutionary pressures that resulted in the observed structural diversity.

## MATERIALS AND METHODS

### Research Specimens

#### Aphrocallistes vastus *and* Rhabdocalyptus dawsoni

Both species were collected by SCUBA at Foley Head, Hotham Sound/Jervis Inlet, British Columbia at *ca*. 25 m depth.



#### Euplectella aspergillum

Specimens of *Euplectella aspergillum* (of Philippine origin) were received as dried skeletons.

#### Monorhaphis chuni

Specimens used in this study were collected from two locations:

1. New Caledonia, near Lifou (Loyalty Island) at a depth of 1905 m during the CALSUB campaign of the IRD 1989.
2. Norfolk Ridge at a depth of 1200 m during the HALIPRO campaign in 1996.

### Sample Preparation

#### A. vastus *and* R. dawsoni

The *A. vastus* sample, depicted in Figs. 3A and B, was soaked in freshwater to remove the residual salts, flash frozen in liquid nitrogen, and lyophilized. All other skeletal material from either *A. vastus* or *R. dawsoni* was soaked in a 5.25% solution of sodium hypochlorite until all of the organic material had been removed. The samples were then washed five times with Milli-Q (Millipore-purified) water, and air-dried at room temperature.

#### M. chuni

All spicule specimens from *M. chuni* were surface cleaned with Milli-Q water and air-dried at room temperature.

## Scanning Electron and Optical Microscopy

Excised portions of the mineralized skeleton of each sponge species were examined by optical microscopy and then mounted on aluminum disks using either conductive carbon tabs, silver paint, or conductive epoxy, depending on the preferred orientation of the sample being examined. Following mounting, all samples were sputter-coated with gold and examined with a Tescan Vega TS 5130MM (Brno, Czech Republic) scanning electron microscope.

## Mechanical Testing

### *Nanoindentation*

Spicule segments were embedded in M-Bond AE-15 (M-Line, Raleigh USA) epoxy resin, sliced into *ca*. 3-mm thick transverse sections using a diamond cutting wheel, and polished with diamond lapping films with particles sizes down to 0.1 μm under a constant flow of fresh water.

For mechanical testing, nanoindentation was performed using a Triboscan nanoindenter system (Hysitron, Minneapolis, MN, USA) and cube-corner tips. Indentations were applied with a high-load transducer permitting applied loads up to 1 N. High loads were mainly selected to ensure damage in the thin-layer region of the spicules. For all indents, the peak load was held constant for 10 s before unloading. Control indentations were made on a fused quartz control slide under similar experimental conditions. After indentation, the samples were sputter-coated with gold and examined with a Tescan Vega TS 5130MM (Brno, Czech Republic) scanning electron microscope (both before and after sonication). The images presented in Fig. 9 are representative of the results obtained.

### *3-Point Bending Tests*

Each of the synthetic glass rods and the giant anchor spicules from *M. chuni* measured *ca*. 5 mm in diameter. The test samples were cut to length with a diamond cutting wheel, surface cleaned with Milli-Q, water, and then air dried at room temperature.

Three-point bending tests were conducted with a 5543 Instron (Norwood, MA, USA) tensile and compression testing machine using a displacement control rate of 2.5 mm/min. A standard three-point bend fixture (Instron) was used and the span was 4 cm.

## Solid-State $^{29}$Si NMR

Solid-state $^{29}$Si NMR experiments were conducted at UCSB on a Bruker (Billerica, MA, USA) DMX-300 spectrometer with a wide-bore 7.0 Tesla superconducting magnet operating at a $^{29}$Si Larmor frequency of 59.6 MHz. The experiments were carried out at room temperature under magic-angle-spinning (MAS) conditions (8 kHz) using a 4-mm double-resonance MAS probehead, on powders prepared from the spicule samples. Single-pulse $^{29}$Si NMR signals were acquired using 1024 transients with a 60 s recycle delay between the transients. $^{1}$H heteronuclear decoupling was applied during acquisition using a SPINAL64 decoupling scheme and a $^{1}$H radio-frequency field strength of 60 kHz. $^{29}$Si signals are referenced to TMS.

## RESULTS AND DISCUSSION

### *Aphrocallistes vastus*

Despite their vast structural diversity (Fig. 1), the smallest of the hexactinellid spicules exhibit a basic design remarkably similar to those encountered in demosponges (such as *Tethya aurantia*; *cf.* [10]),

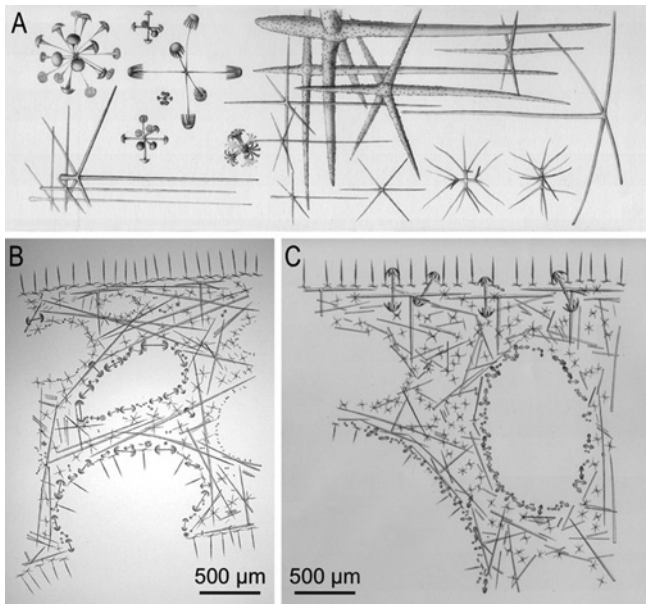


**FIGURE 1** (A) Structural diversity and (B,C) regiospecificity of hexactinellid spicules (adapted from [5,34]).

consisting of a central axial filament surrounded by concentric lamellae of consolidated silica nanoparticles. When these spicules are fractured, like those from demosponges, they fail catastrophically without any indication of the presence of structural boundaries (Fig. 2A) *via* the uninterrupted propagation of a single dominant crack.

In the skeletal system of *Aphrocallistes vastus* (Fig. 3A), for example, the outer surface is almost completely covered with numerous such spicules that are held in place by the syncytium and are positioned perpendicular to the surface (Figs. 3B–D) [5]. While these spicules do exhibit the unique three-axis symmetry characteristic of hexactinellids, the rays are unequally developed, resulting in the formation of the characteristic pinnule (sword shaped) spicules shown in Fig. 3D. Beneath this outer layer of protective spicules is the main skeletal lattice [4,5]. This skeletal lattice consists of an intricate network of fused six-rayed spicules (hexactines), each of which measures *ca*. 200 μm in length (Fig. 3G).

These spicules are fused together at the end of each ray in such a manner that results in the formation of a rigid honeycomb-like architecture (Figs. 3E, F) and can exhibit a remarkable degree of ordering when viewed in cross-section, with many of the constituent spicules fused at right angles with respect to one another (Figs. 4A, B).

The organic scaffold (consisting of the six-rayed axial filaments) is not continuous throughout the lattice, although it may overlap at the points of fusion between two neighboring spicules (Figs. 4C–E).



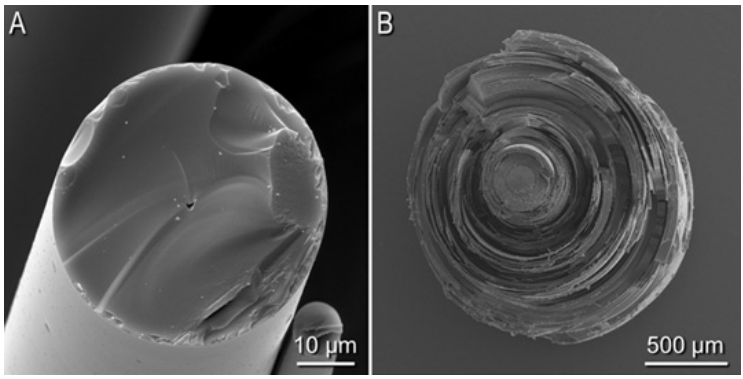


**FIGURE 2** Failure modes of (A) nonlaminated and (B) laminated spicules. (A) is from the demosponge *Tethya aurantia* and (B) is from the hexactinellid *Monorhaphis chuni*.

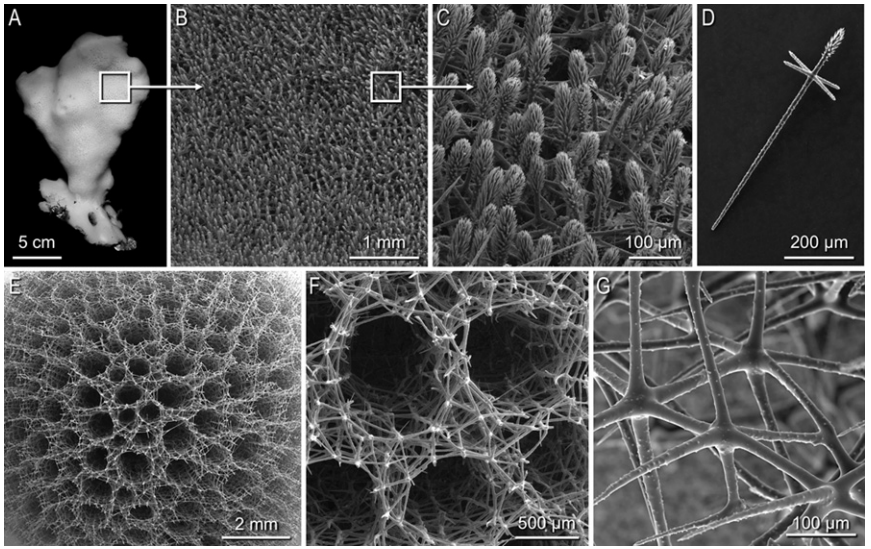


**FIGURE 3** (A–D) External armament of *Aphrocallistes vastus* (A). (B, C) The external surface of *A. vastus* is completely covered with (D) protective pinnule spicules, each of which measures *ca.* 650 µm in length. (E-G) Primary skeletal system of *Aphrocallistes vastus*. Various progressively magnified views of the honeycomb-like skeletal network of *A. vastus*, which is composed entirely of fused hexactines. In this series of images, the pinnule spicules (shown in B–D) have been removed.



This observation suggests that the ray length of the constituent spicules are largely synthesized in their entirety prior to incorporation into the lattice. While this may be the case, at the points of spicule fusion there are no indications of structural boundaries, indicating that the lattice formation is largely a continuous process and that the process of spicule cementation may occur as a continuation of the lateral growth of the constituent spicules [5]. In *A. vastus*, as is the case for many other closely related hexactinellid sponges of the order Hexactinosida, the incorporation and direct fusion of small spicules into a rigid skeletal lattice is a common and characteristic design strategy [4,5]. The maximum length of all spicules in these species does not exceed a few millimeters in length. Thus, a design strategy similar to that observed in the demosponge spicules, coupled with the hierarchical assembly and cementation described above, apparently is sufficiently robust to survive the loading regimes experienced by these species.

### *Rhabdocalyptus dawsoni*

From a structural and mechanical perspective, the most remarkable of the hexactinellid spicules are the significantly larger ones that form the basis of the skeletal system of many species such as *Rhabdocalyptus dawsoni* (Fig. 5A). These spicules, which lie spatially isolated from one another in *R. dawsoni*, can frequently measure up to a centimeter or more in length (Fig. 5B) and are characterized by their distinctive laminated architecture. These spicules consist of a solid featureless central cylinder of silica that encases the axial filament and is surrounded by concentric lamellae of consolidated silica nanoparticles

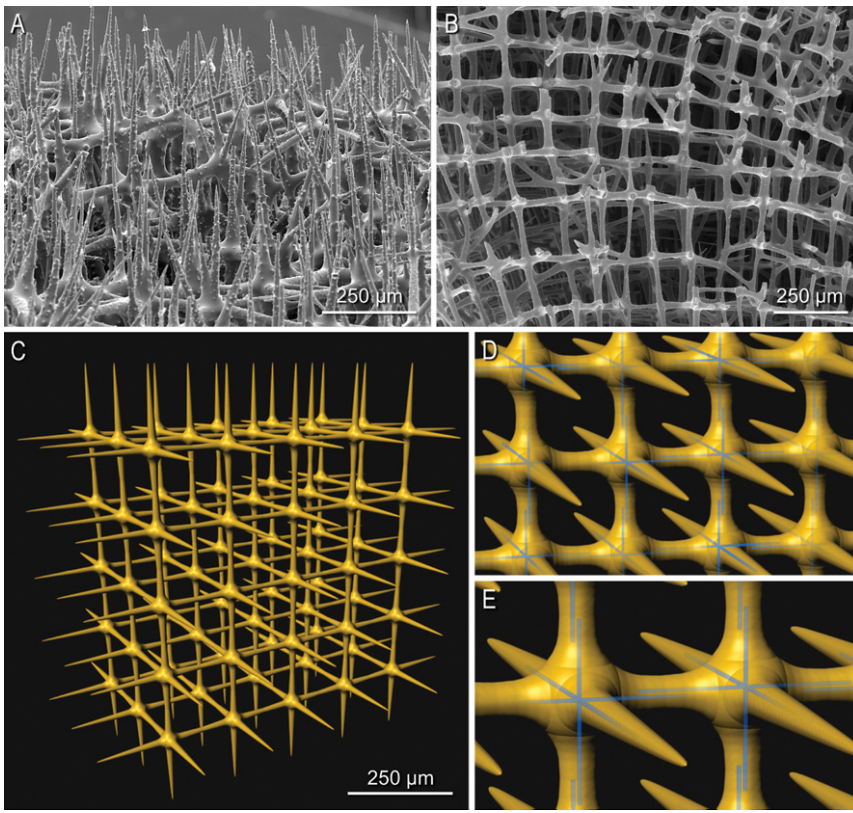


**FIGURE 4** (A) Exterior and (B) interior views of the highly ordered network of fused hexactines in *Aphrocallistes vastus*. (C–E) Three-dimensional structural rendering of the location of the organic scaffold (shown in blue) within the skeletal lattice of *A. vastus*. Data used for the 3-D renderings were obtained from [5] and our optical microscopy studies.

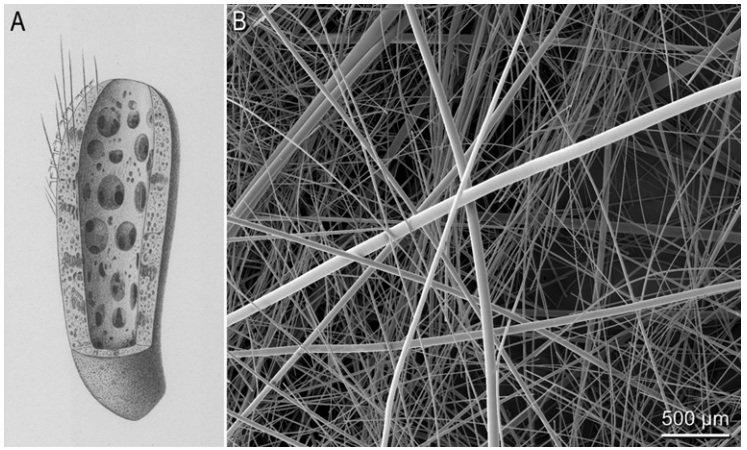


**FIGURE 5** Skeletal system of *Rhabdocalyptus dawsoni*. (A) Illustration of the North Eastern Pacific hexactinellid *R. dawsoni*, shown approximately life-size and (B) its mineralized skeletal system consisting largely of laminated needle-like spicules. ((A) adapted from [5]).



and organic thin interlayers, forming a microlaminate (*cf*. Figs. 2B, 12B, C).

The fact that longer cylinders of a given radius are less mechanically robust is intuitive, but to illustrate the point: consider two cylinders of equal radii but having different lengths, both fixed at one of their ends. If a load is applied orthogonal to the central axis of each cylinder, then the cylinders will be perturbed from their linear shape and the bending about the fixed end will either be balanced by a reactionary force or the cylinder will begin to fail. The cylinders will flex more with increasing distance of the applied force from the fixed end. Because longer spicules can receive a load further from its fixed point, they can be subjected to a greater strain per unit force applied and therefore have a greater chance of failure. Furthermore, surface abrasions and other defects lead to premature failure because they act as sites for strain concentration and instigate the formation of cracks. In nonlaminated spicules, a single crack has a high probability of resulting in catastrophic failure. Since longer spicules can accumulate more abrasions and surface defects, a laminated architecture is an effective means by which to inhibit crack propagation.

When examined in cross-section, there is a distinct reduction in silica layer thickness from the spicule core to its periphery. The thinner outer layers significantly limit the depth of crack penetration into the spicule interior, effectively increasing the damage tolerance of this

composite structure [16–21]. In addition, the number of silica layers increases with increasing spicule length, with the largest laminated spicules from *R. dawsoni* containing 15 or more separate silica layers. While it is tempting to attribute the reduction in layer thickness that accompanies spicule diameter to the deposition of a fixed volume of silica per layer (which would result in a continuous reduction in layer thickness as a function of spicule radial growth), these trends are not typically observed.

The benefits of damage tolerance and reduced sensitivity to flaws imparted by the laminated structure can be predicted from established models of fracture mechanics for the two limiting cases shown in Fig. 6 [23]. In the first, the material is modeled as a series of weakly bonded brittle plates, each of thickness $t$, with flaws of length $c$, and a fracture toughness $K_c$. Provided that the dominant crack (consisting, say, of several broken plates) is sufficiently blunted by the organic interlayer to completely mitigate the associated stress intensity, renucleation can occur only when the stress in the intact layers reaches its intrinsic strength: $\sigma_o = K_c/1.12\sqrt{\pi c}$. Since, in this limit, the stress in the intact layers is uniform, the fracture stress (in



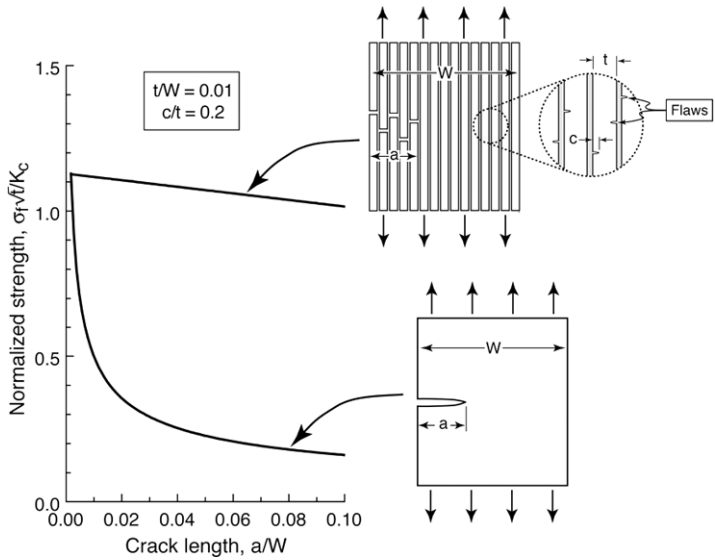


**FIGURE 6** Normalized strength *vs*. crack length for laminated and monolithic materials. The thickness of the organic interlayers (highlighted in gray) is exaggerated in the illustration.

normalized form) becomes $\sigma_f\sqrt{t}/K_c = (1-a/W)\sqrt{t/\pi c}/1.12$. In the second case, the material is treated as a homogeneous monolithic body, also with fracture toughness $K_c$. The corresponding fracture stress is $\sigma_f\sqrt{t}/K_c = \sqrt{t/W}/1.12\sqrt{\pi a/W}$. Comparisons of flaw sensitivities of the two structures are presented in Fig. 6, for the case wherein $t/W = 0.01$ (a laminate with 100 layers) and an intrinsic flaw size $c/t = 0.2$. The number of layers selected for this model is arbitrary, but lies well between two of the cases discussed in this report (*R. dawsoni* and *M. chuni*). Clearly, the effects of the laminated structure on spicule strength are significant. For instance, for a crack comprising five broken layers ($a/t = 5$ and hence $a/W = 0.05$), the retained strength of the weakly bonded laminate is about five times that of the monolithic body with the same crack dimension. The behavior of the spicules is expected to lie between these two limits, depending on the extent to which the organic interlayers mitigate the near-tip stresses.



## *Monorhaphis chuni*

A modification to the basic laminated spicule design strategy described in *R. dawsoni* is observed in *Monorhaphis chuni*. In this species, and in stark contrast to all other genera of sediment dwelling hexactinellids (Fig. 7), skeletal support and benthic anchoring is provided by a single monolithic anchoring spicule measuring up to three meters long and almost one centimeter thick [22], a portion of one such spicule is shown in Fig. 8A.

Presumably as a consequence of its large size and in response to the local environmental conditions (prevailing currents, etc.), the spicule develops a natural curvature (Figs. 8A, B). This creates spicule zones of maximum tension and compression and is accompanied by a distinct asymmetry in silica layer thickness; the thinnest exterior layers under maximum tension help limit the depth of crack penetration, while the thickest exterior layers prevent buckling in the zone of maximum compression (Figs. 8C–F) [23]. In many instances, large spicules (greater than 2 m in length and containing nearly 500 separate silica layers) develop an elliptical cross-section, with the major axis of the ellipse coinciding with the direction of curvature (Figs. 8B, C).

The layer asymmetry observed in *M. chuni* is unique to this species and is most likely a stress-induced response to the predominantly unidirectional bending regimes of this monolithic structure, thus, raising intriguing questions as to the sensory and silica deposition regulatory mechanisms that result in this remarkable design strategy. Despite its exceptional rarity and deep dwelling nature (frequently encountered

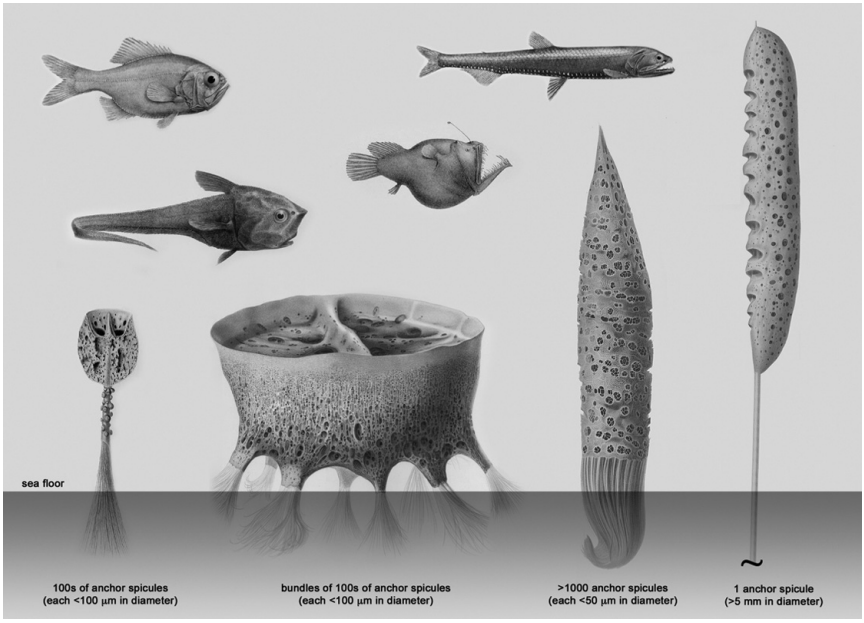


**FIGURE 7** Holdfast diversity in hexactinellid sponges. In stark contrast to other sediment-dwelling hexactinellid sponges (from left to right: *Hyalonema, Chaunangium, Semperella), Monorhaphis* (far right) is anchored into the sea floor by a single giant spicule measuring up to 3 m long and nearly 1 cm thick (adapted from [4,5,35]).



at depths exceeding 2000 m), the giant anchor spicule from *M. chuni* has proven to be an exceptionally useful model system for investigating a wide range of chemical, mechanical, and ultrastructural properties of laminated spicules, mainly due to its unusually large size [24–26]. No other described species of sponge synthesizes spicules that are even remotely comparable in dimensions with that encountered in this species. This attribute makes it an ideal research subject for mechanical and compositional studies of biosilica, using techniques that are not readily applicable to smaller spicules. For instance, using Raman spectroscopy for chemical mapping of the spicules from this species [25], it was revealed for the first time that the organic interlayers are protein-rich, based on their characteristic C-H stretch and amide vibrational signatures (Fig. 8G).

Additional information obtained from high load nanoindentation studies reveal the remarkable energy-dissipating properties of this laminated architecture [23]. Nanoindentation results demonstrate

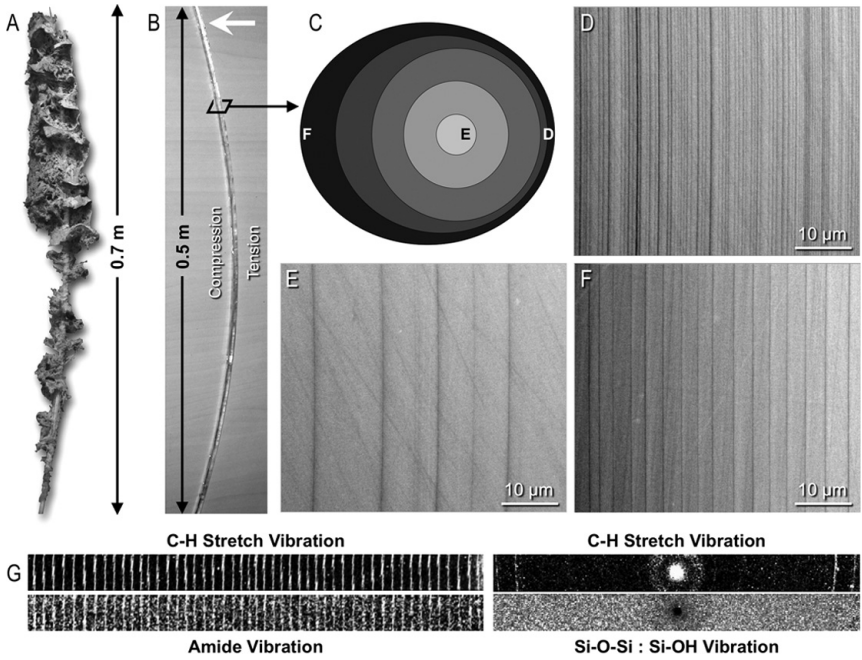


**FIGURE 8** (A) Design features of the giant anchor spicule of *Monorhaphis chuni* (sponge photo adapted from [5]). Unidirectional spicule curvature results in asymmetrical strain accumulation. The large white arrow in (B) indicates the direction of bending, resulting in specific zones under tension and compression. Cross-sections through the spicule shown in (B) [(C) graphical representation and (D–F) environmental SEM images] reveal the accompanying asymmetrical silica deposition. (E) The difference in silica layer thickness from one side of the spicule to the other (in the direction of loading) is nearly 6-fold [(D) *ca.* 500 nm per layer (F) *ca.* 3 μm per layer]. (E) The thickest layers, immediately surrounding the central cylinder, measure *ca.* 10 μm thick. (G) Raman chemical mapping of *M. chuni* spicule cross-sections. C-H stretch (2937 $cm^{-1}$) and amide (1655 $cm^{-1}$) vibrations through the spicule cortex confirm that the organic interlayers are protein-rich. C-H stretch vibrations (2937 $cm^{-1}$) around the axial filament confirm the presence of extra-axial filament occluded organics within the biosilica (Si-O-Si at ~800 $cm^{-1}$ and Si-OH at 975 $cm^{-1}$) and an accompanying decrease in the degree of silica condensation. (B) and (G) adapted from [25], used with permission from Materials Research Society. (D) and (F) adapted from [23], used with permission from Wiley.

that when compared with the monolithic material encountered in the central cylinder region immediately surrounding the axial filament, the laminated architecture effectively inhibits crack initiation from

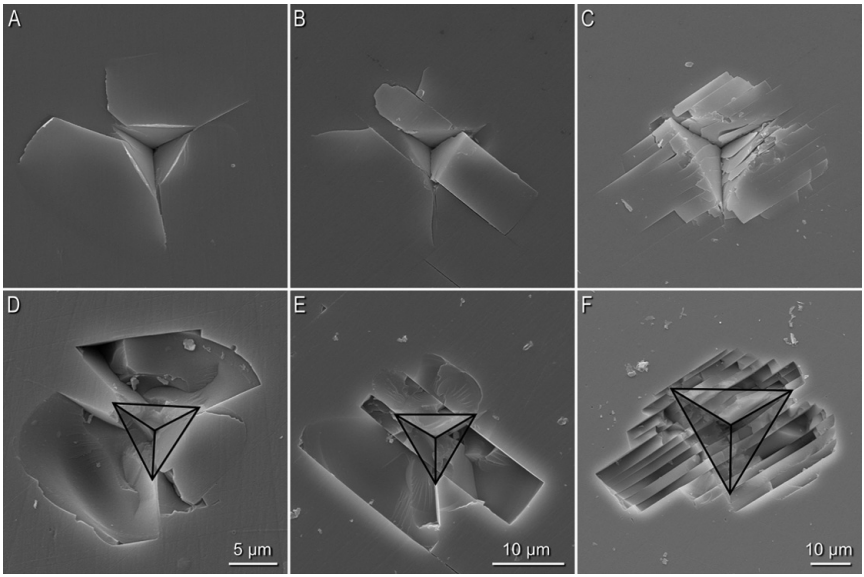


**FIGURE 9** Regiospecific indentation fracture in the giant anchor spicule of *Monorhaphis chuni*. SEM images illustrating the crack morphology and extent of damage created by (A,D) indentation before (upper) and after (lower) sonication in the monolithic core, (B,E) the thick layer region immediately surrounding the monolithic core, and (C,F) the region of minimum layer thickness near the spicule exterior on the side of tensile loading of the spicule shown in Fig. 8B; core (non-laminated) region, 100 mN (A) before and (D) after sonication; *thick layer* region, 200 mN indent, (B) before and (E) after sonication; *thin layer* region, 200 mN indent, (C) before and (F) after sonication. The black triangle in (D–F) represent the locations of the initial impressions in (A–C), respectively. (A) and (D) adapted from [23], used with permission from Wiley.



the corners of the indents (Fig. 9). All of the applied energy appears to be dissipated locally with no net effect on the macroscopic structural integrity of the spicule. In addition, the extent to which the damage field extends beyond the site of indentation critically depends on the relative distance between the organic interlayers [23].

Cross-sections through a fractured spicule (Figs. 10A, B) clearly reveal the crack-stopping properties of the organic interlayers, which exhibit a distinctive stair step-like crack pattern resulting from multiple sequential arrests and renucleations during crack propagation. In addition to the crack deflecting capabilities of the organic interlayers, a propagating crack can even be confined to a specific radial depth as it travels parallel to the long axis of the spicule in a helical

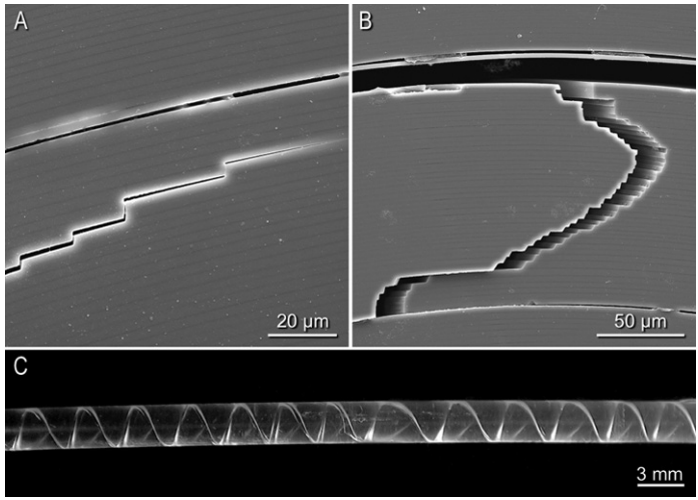


**FIGURE 10** Fracture dynamics of laminated spicules from *Monorhaphis chuni*: (A,B) Cracks propagating through a damaged anchor spicule from *M. chuni* exhibit a distinct step-mode, clearly illustrating the crack-deflecting properties of the organic interlayers. (C) In some instances, rather than propagating through the multilayer architecture, cracks can be spatially restricted to a specific radial depth of the spicule and can travel parallel to its long axis in a helical fashion (photograph of a fractured spicule illuminated end-on). (A) adapted from [27], used with permission from AAAS. (B) adapted from [23], with permission from Wiley.



fashion, fracturing only the silica layers immediately adjacent to the crack trajectory (Fig. 10C). The energy dissipated in this damage mode is significant if one considers that a 2-m long spicule measuring 5 mm in diameter can propagate a crack over 1 m long through the spicule without any significant loss in its structural integrity.

To investigate how the observed micromechanical properties revealed in the nanoindentation studies affect the global macromechanical properties of the giant anchor spicule of *M. chuni*, we conducted a series of three-point bending tests (Fig. 11) on these spicules, similar measurements of which have been reported elsewhere [21,24]. These results were compared with those obtained from duplicate tests performed on monolithic glass rods of similar dimensions (both *ca.* 5 mm in diameter) and similar moduli (36 GPa for the synthetic glass rod and 23 GPa for the spicule). The fracture stress (sometimes referred to as the "modulus of rupture") was calculated from the resulting load–displacement curves, using the assumption that the

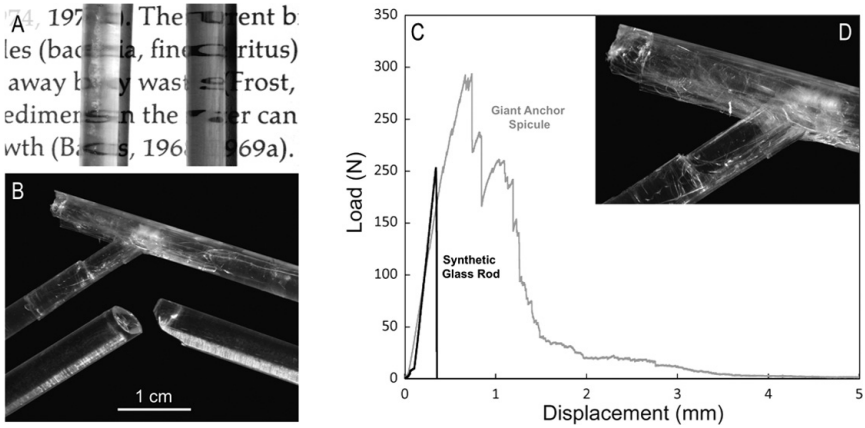


**FIGURE 11** Fracture dynamics of the giant anchor spicule of *Monorhaphis chuni* and a synthetic glass rod of similar diameter and modulus: (A) Photograph illustrating the 5-mm diameter samples used in this study highlighting their optical transparency (spicule, left; synthetic glass rod, right). (B) Photographs of the same structures following failure from a three-point bending test (spicule, upper; synthetic glass rod, lower) and (C) their corresponding load *vs*. displacement curves. (D) A higher magnification view of the fractured spicule showing clear delamination of the silica layers.



samples behave elastically. Thus, the maximum stress on a cylindrical beam in bending is: $\sigma = Mr/I$, where $r$ is the radius of the cylinder, $I$ is the moment of inertia, and $M$ is the bending moment. The largest bending moment, $M$, occurs in the middle of the span so that: $M = PL/4$, where $P$ is the load and $L$ is the span length. For a cylinder, the moment of inertia, $I$, is: $I = \pi r^4/4$, where $r$ is the cylinder radius. The stress at fracture, $\sigma_{fb}$, for a cylinder can be defined as: $\sigma_{fb} = P_f L/\pi r^3$, where $P_f$ is the load at fracture.

The elastic modulus, $E$, can also be found from our three-point bending tests. The maximum deflection, $v$, occurs at the midpoint and is: $v = PL^3/48EI$; thus, the modulus can be found using: $E = L^3/48I(dP/dv) = L^3/12\pi r^4(dP/dv)$, where the quantity in parentheses is the linear slope of the load-displacement curve. Despite the higher modulus of the synthetic glass rods (Fig. 11C), the yield strength is 50% higher for the giant anchor spicules, with a corresponding 45% increase in fracture stress, $\boldsymbol{\sigma_{fb}}$ (164 MPa for the monolithic glass rod and 237 MPa for the giant anchor spicule), and a ten-fold increase in toughness (calculated from the areas under the load *vs*. displacement curves).

## *Euplectella aspergillum*

In addition to their remarkable mechanical properties, the hexactinellids are also well known for the ability to form extremely complex, hierarchically ordered, robust skeletal networks from their constituent spicules [27,28]. One such example is *Euplectella aspergillum* (Fig. 12A), a common deep-sea sediment-dwelling hexactinellid from the Western Pacific [4,5]. As in the case of spicule fusion observed in *A. vastus*, the skeletal system of *E. aspergillum* also consists of a rigid skeletal lattice, although the design strategies implemented in its construction are quite different. While the basic structural unit from which the skeletal framework of *A. vastus* is constructed, is the

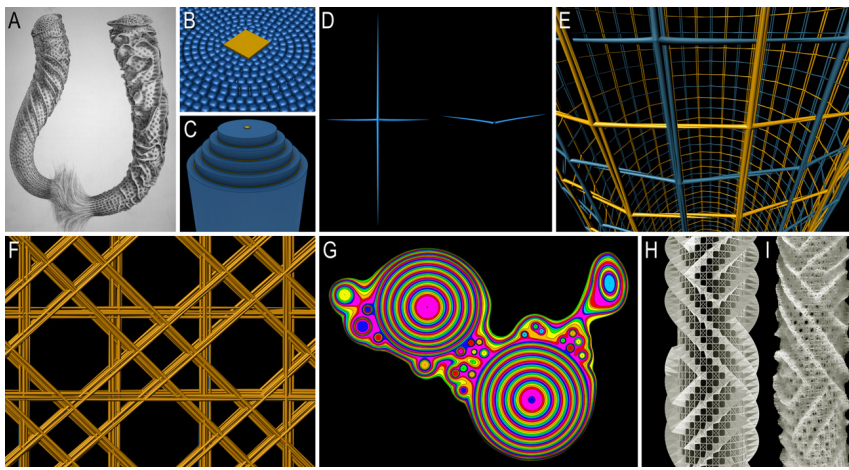


**FIGURE 12** Hierarchical organization of the skeletal lattice of *Euplectella aspergillum*. (A) Preserved specimens of *E. aspergillum* clearly illustrating the cylindrical bodyplan, the external ridge system, the holdfast apparatus, and the terminal sieve plate. Each of (D) the nonplanar cruciform (stauractine) spicules consists of a central proteinaceous axial filament surrounded by (B,C) concentric lamellae of consolidated silica nanoparticles and organic interlayers. These are combined into (E) two interpenetrating square lattices (one shown in blue, one in yellow), which are further reinforced with (F) bundled spicules organized vertically, horizontally, and diagonally forming alternating open and closed squares measuring 2.5–3 mm in width. (G) The resulting checkerboard-like configuration is consolidated with a laminated cement (color-coded cross-section to highlight the laminated architecture) and (H) covered by an alternating network of external ridges. The two largest laminated spicules in (G) are the stauractines shown in (D). A photograph of the specimen after which (H) was modeled is shown in (I). All images adapted from [28], used with permission from Elsevier.

hexactine (Fig. 3), the framework of the skeletal lattice of *E. aspergillum* is composed of stauractine (non-planar cruciform) spicules (Fig. 12D). Like the spicules from *R. dawsoni*, these spicules consist of a central proteinaceous axial filament surrounded by concentric lamellae of consolidated silica nanoparticles and organic interlayers forming a laminated composite (Figs. 12B, C) [27,28].

Two intersecting grids of these non-planar cruciform spicules define a locally quadrate, globally cylindrical, skeletal lattice that provides the framework, onto which other skeletal constituents are deposited, as shown in Fig. 12E [27,28]. The grids are supported by bundles of spicules that form vertical, horizontal, and diagonally ordered struts covering the resulting square openings in an alternating checkerboard-like manner, as depicted in Fig. 12F. Each strut consists of a wide size range of individual spicules, ranging from 5 to 50 μm in diameter and of variable length. These struts help stabilize the lattice and provide additional mechanical support [16], forming a series of nearly uniform quadrate meshes averaging 2.5–3 mm in size. The incorporation of diagonal bracings as part of this configuration is essential for supporting the bending, shear, and torsional loads experienced by the skeletal lattice [29]. The overall cylindrical lattice is capped at its upper end by a terminal sieve plate and rooted into the sea floor at its base by a flexible cluster of barbed fibrillar anchor spicules (Fig. 12A) [30,31]. External diagonally oriented spiral ridges that extend perpendicular to the surface further strengthen the lattice and likely help prevent ovalization during lateral compression (Figs. 12H, I). A secondarily deposited laminated silica matrix (Fig. 12G) that cements the structure together additionally reinforces the resulting skeletal mass. At higher magnification, it can be seen clearly that the consolidating silica cement precisely follows the contours of the underlying spicules, apparently enhancing the strength of this fiber-reinforced composite, the structure of which is similar to armored concrete.

It is important to note that the mode of skeletal consolidation follows the general design principle also exhibited in the dominant constituent spicules themselves. The significance of this observation is that, due to its laminated architecture, the cement itself is able to dissipate a significant amount of energy during loading through crack deflection at the organic interlayers, while simultaneously distributing the applied load over the entire network of underlying spicules.

## $^{29}$Si NMR STUDIES

The mechanical properties of hierarchically structured materials such as sponge spicules are governed by both their molecular architectures

as well as by the meso- and micro-structural motifs employed by the different sponge species, apparently selected as adaptations to their environments. As the spicules are highly siliceous, at a molecular level their structures are primarily governed by the relative concentrations of so-called "$Q^n$" silicon species (integer $n \leq 4$), which refer to Si atoms bonded covalently to four bridging oxygen atoms, $n$ of which are bonded to other Si atoms [32]. For example, $Q^4$ silicon species are covalently bonded to four other Si atoms *via* oxygen atoms; these correspond to fully condensed moieties, the relative concentration of which corresponds to the extent of cross-linking of the siliceous matrix. Similarly, in $Q^3$ silicon species Si atoms are bonded *via* bridging oxygen atoms to three other Si atoms and, thus, are incompletely condensed. By determining the relative fractions of the different $Q^n$ silicon species, the molecular structures of spicules associated with different sponge species can be compared and correlated with their different bulk mechanical properties.



Solid-state $^{29}$Si nuclear magnetic resonance (NMR) spectroscopy is sensitive to the local bonding environments of $^{29}$Si species and can be

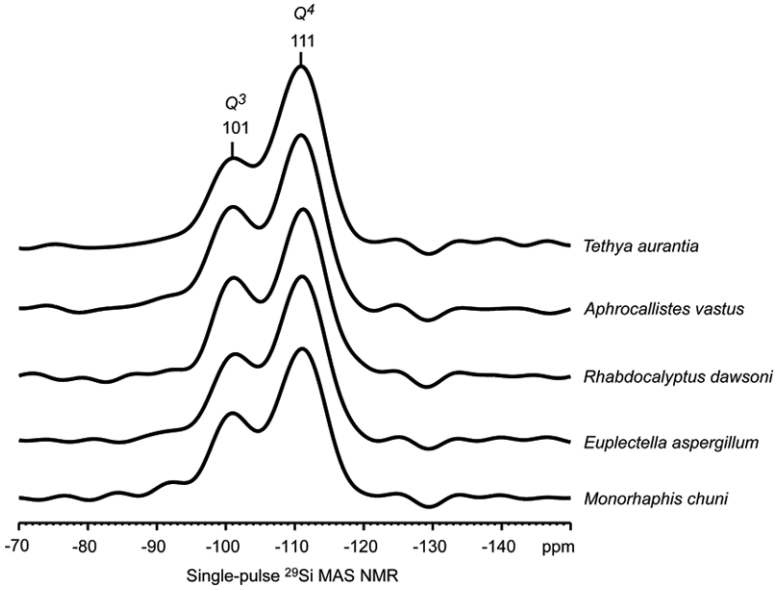


**FIGURE 13** Room-temperature single-pulse $^{29}$Si MAS NMR spectra of ground spicules from the sponge species indicated. These data reveal that regardless of the mode of skeletal construction (and the architecture of the constituent spicules), there are no significant distinguishable differences in the degree of silica condensation between the spicules of these five species.

used to quantify the relative concentrations of $Q^n$ $^{29}$Si species in spicules from different sponge species [10]. Single-pulse $^{29}$Si NMR spectra acquired under conditions of magic-angle sample spinning show two broad signals centered at 101 and 111 ppm, respectively, which correspond to the $Q^3$ and $Q^4$ $^{29}$Si species (Fig. 13). The absence of downfield signals (<100 ppm) in the spectra reveal no detectable quantities of $Q^0$, $Q^1$, or $Q^2$ species, from which it is established that all of the silica is present in a highly (but incompletely) cross-linked structure. Furthermore, the broad $^{29}$Si lineshapes indicate that broad distributions of $Q^3$ and $Q^4$ $^{29}$Si sites are present, consistent with an amorphous, glass-like structure of the condensed silica networks. Deconvolution and integration of the quantitative single-pulse $^{29}$Si NMR spectra in Fig. 13 establish similar extents of cross-linking, $Q^4/(Q^3+Q^4)=0.65$ for all of the spicules measured. This indicates that molecular structures of the $^{29}$Si matrices are similar for all of the species investigated, suggesting that observed differences in sponge spicule mechanical properties may be attributed to differences in macroscopic (*e.g.*, laminated *vs*. non-laminated) architectures and not from significant variability in the degree of silica condensation.



## ADDITIONAL OBSERVATIONS

Recent studies investigating early larval development of the hexactinellid *Oopsacas minuta* reveal that their syncytial architecture is secondarily derived, arising from the 32-cell stage, after which micromere fusion results in the formation of a syncytial mass [33]. These results are significant in that they suggest that the ancestral metazoan group that gave rise to the Porifera was cellular and not syncytial, thus, raising intriguing questions as to the selective pressures that may have favored the evolution of the unique hexactinellid body plan. One possible answer to this question can be found by exploring the environment to which the hexactinellids have adapted through the course of evolution. While virtually all other sponge species occur on solid substrates, the hexactinellids are unique in that they have evolved the capacity to colonize soft sediments [4,5]. One unifying feature of the sediment-dwelling hexactinellids is the evolution of a holdfast apparatus, which typically consists of basalia (anchor spicules) measuring tens of centimeters in length (Fig. 7). These long anchor spicules are essential for soft sediment colonization and hexactinellids lacking basalia (Fig. 3) are confined to more solid substrates. As discussed above, only a syncytial body plan (Fig. 14) could facilitate the synthesis of spicules greater than a few millimeters in length. Consequently, it is

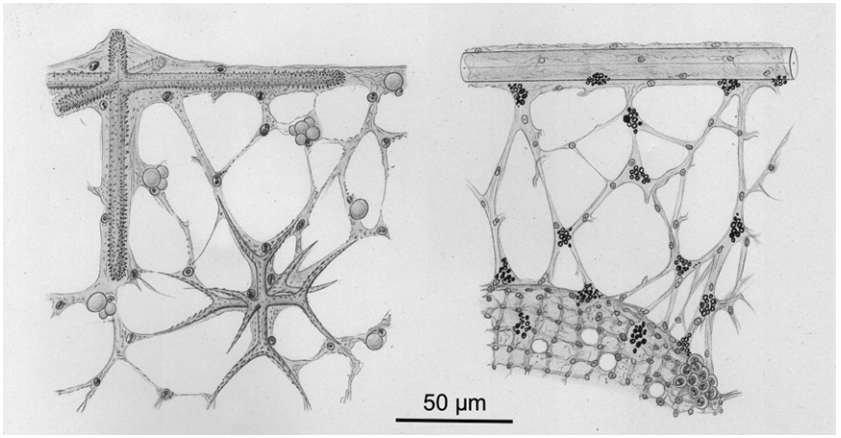


**FIGURE 14** Illustration of the hexactinellid syncytial architecture and their associated spicules (adapted from [5]).



reasonable to suggest that the syncytial architecture evolved in this group of early sponges in habitats of reduced solid substrate availability, which characterizes the predominantly deep-sea habitats in which the majority of hexactinellids now survive [4,5].

## SUMMARY

As we have seen from these studies, the siliceous skeletal systems of sponges are well suited to meet the structural needs of each species. The following summarizes the general design strategies observed in the siliceous skeletal elements of the Porifera, as discussed in this report:

1) Spicules greater than a few millimeters in length exhibit unique laminated architectures, which effectively retard crack propagation.
2) The number of laminate layers increases with spicule length and typically decreases in thickness radially outward from the core.
3) The mode of spicule consolidation, when present, follows the general design schemes present in the dominant constituent spicules; laminated spicules use a laminated cement, nonlaminated spicules use a nonlaminated cement.
4) Large spicules confronting unidirectional bending regimes exhibit a unique vectorially graded architecture for enhanced fracture resistance.

Additional research into the structure-function relationships of these materials is expected to provide important new understanding and inspiration for the fabrication of a new generation of complex, robust, hierarchically ordered, fracture-resistant three-dimensional composites.

## ACKNOWLEDGMENTS

We thank Frank Zok, J. Herbert Waite, Shane Anderson, Nemil Vora, Corey Hardin, Amy Butros, and Armand Kuris for helpful suggestions. DK and NV were supported by a University of California, Riverside Undergraduate Research Grant (#A01009-07431-40-43). JCW and DEM were supported by grants from NASA (NAG1-01-003 and NCC-1-02037); the Institute for Collaborative Biotechnologies, Army Research Office (DAAD19-03D-0004); the NOAA National Sea Grant College Program, U.S. Department of Commerce (NA36RG0537, Project R/MP-92); and the MRSEC Program of the National Science Foundation (DMR-00-8034). PF acknowledges support by the Max Planck Research Award from the Alexander von Humboldt Foundation. BFC acknowledges support from the U.S. National Science Foundation (grant CBET-0829182).



## REFERENCES

[1] Garrone, R., Simpson, T. L., and Pottu-Boumendil, J., Ultrastructure and deposition of silica in sponges, in *Silicon and Siliceous Structures in Biological Systems*, T. L. Simpson and B. E. Volcani (Eds.) (Springer-Verlag, New York, 1981), pp. 495–525.
[2] Hartman, W. D., Form and distribution of silica in sponges, in *Silicon and Siliceous Structures in Biological Systems*, T. L. Simpson and B. E. Volcani (Eds.) (Springer-Verlag, New York, 1981), pp. 453–493.
[3] Schulze, F. E., *Trans. R. Soc Edinburgh.* **29**, 661–673 (1880).
[4] Schulze, F. E., 1887. *Report on the Hexactinellida Collected by H. M. S. Challenger During the Years 1873–1876*, Volume **XXI** (Neill and Company, Edinburgh).
[5] Schulze, F. E., Hexactinellida, in *Scientific Results of the German Deep-Sea Expedition with the Steamboat, Valdivia 1898–1899*, C. Chun (Ed.) (Verlag Gustav Fischer, Jena, Germany, 1904).
[6] Schulze, F. E., Zur Histologie der Hexactinelliden, *Sitz. Ber. K. Pr. Akad. Wiss. Berlin.* **14**, 198–209 (1899).
[7] Mackie, G. O. and Singla, C. L., *Phil. Trans. R. Soc. Lond.* **301**, 365–400 (1983).
[8] Uriz, M. J., Turon, X., and Becerro, M. A., *Cell Tiss. Res.* **301**, 299–309 (2000).
[9] Schwab, D. W. and Shore, R. E., *Nature* **232**, 501–502 (1971).
[10] Weaver, J. C., Pietrasanta, L. I., Hedin, N., Chmelka, B. F., Hansma, P. K., and Morse, D. E., *J. Struct. Biol.* **144**, 271–281 (2003).
[11] Reiswig, H. M., *Can. Biol. Mar.* **12**, 505–514 (1971).
[12] Simpson, T. L., (Springer-Verlag, New York, 1984).
[13] Simpson, T. L., Langenbruch, P. F., and Scaleraliaci, L., *Zoomorphology* **105**, 375–382 (1985).

[14] Weaver, J. C. and Morse, D. E., *Microsc. Res. Techniq.* **62**, 356–367 (2003).
[15] Leys, S. P., *Microsc. Res. Techniq.* **62**, 300–311 (2003).
[16] Clegg, W. J., Kendall, K., Alford, N. M., Button, T. W., and Birchall, J. D., *Nature* **347**, 455 (1990).
[17] Sarikaya, M., Fong, H., Sunderland, N., Flinn, B. D., Mayer, G., Mescher, A., and Gaino, E., *J. Mater. Res.* **16**, 1420–1428 (2001).
[18] Chai, H. and Lawn, B. R., *Acta Mater.* **50**, 2613–2625 (2002).
[19] Seshadri, M., Bennison, S. J., Jagota, A., and Saigal, S., *Acta Mater.* **50**, 4477–4490 (2002).
[20] Fratzl, P., Gupta, H. S., Fischer, F. D., and Kolednik, O., *Advanced Materials* **19**, 2657–2661 (2007).
[21] Muller, W. E. G., Wang, X. H., Kropf, K., Ushijima, H., Guertsen, W., Eckert, C., Tahir, M. N., Tremel, W., Boreiko, A., Schlossmacher, U., Li, J. H., and Schroder, H. C., *Journal of Structural Biology* **161** (2), 188–203 (2008).
[22] Miserez, A., Weaver, J. C., Thurner, P. J., Aizenberg, J., Dauphin, Y., Fratzl, P., Morse, D. E., and Zok, F. W., *Advanced Functional Materials* **18**, 1241–1248 (2008).
[23] Chun, C., *Aus den Tiefen des Weltmeers: Schilderungen von der Deutschen Tieffee-Expedition*, (Gustav Fischer Verlag, Jena, 1900).
[24] Levi, C., Barton, J. L., Guillemet, C., Lebras, E., and Lehuede, P. J., *Mater. Sci. Lett.* **8**, 337–339 (1989).
[25] Woesz, A., Weaver, J. C., Kazanci, M., Dauphin, Y., Aizenberg, J., Morse, D. E., and Fratzl, P., *Journal of Materials Research* **21**, 2068–2078 (2006).
[26] Müller, W. E. G., Eckert, C., Kropf, K., Wang, X., Schloßmacher, U., Seckert, C., Wolf, S., Tremel, W., and Heinz, S., *Cell and Tissue Research* **329**, 363–378 (2007).
[27] Aizenberg, J., Weaver, J. C., Thanawala, M. S., Sundar, V. C., Morse, D. E., and Fratzl, P., *Science* **309**, 275–278 (2005).
[28] Weaver, J. C., Aizenberg, J., Fantner, G. E., Kisailus, D., Woesz, A., Allen, P., Fields, K., Porter, M. J., Zok, F. W., Hansma, P. K., Fratzl, P., and Morse, D. E., *Journal of Structural Biology* **158**, 93–106 (2007).
[29] Deshpande, V. S., Ashby, M. F., and Fleck, N. A., *Acta Mater.* **49**, 1035–1040 (2001).
[30] Sundar, V. C., Yablon, A. D., Grazul, J. L., Ilan, M., and Aizenberg, J., *Nature* **424**, 899–900 (2003).
[31] Aizenberg, J., Sundar, V. C., Yablon, A. D., Weaver, J. C., and Chen, G., *Proc. Natl. Acad. Sci. USA* **101**, 3358–3363 (2004).
[32] Engelhardt, G. and Michel, D., *High-Resolution Solid-State NMR of Silicates and Zeolites*, (Wiley, Chichester, 1987).
[33] Leys, S. P., Cheung, E., and Boury-Esnault, N., *Integrative and Comparative Biology* **46**, 104–117 (2006).
[34] Iijima, I., *The Hexactinellida of the Siboga Expedition*, (Leiden, Brill, 1926).
[35] Günther, A., *Report on the Deep-Sea Fishes Collected by H. M. S. Challenger During the Years 1873–1876*, Volume **XXII**. (Neill and Company, Edinburgh, 1887).